Early detection of neuropathophysiology using diffusion-weighted magnetic resonance imaging in asymptomatic cats with feline immunodeficiency viral infection

Daniel S. Bucy · Mark S. Brown · Helle Bielefeldt-Ohmann · Jesse Thompson · Annette M. Bachand · Michelle Morges · John H. Elder · Sue VandeWoude · Susan L. Kraft

Abstract HIV infection results in a highly prevalent syndrome of cognitive and motor disorders designated as HIV-associated dementia (HAD). Neurologic dysfunction resembling HAD has been documented in cats infected with strain PPR of the feline immunodeficiency virus (FIV), whereas another highly pathogenic strain (C36) has not been known to cause neurologic signs. Animals experimentally infected with equivalent doses of FIV-C36 or FIV-PPR, and uninfected controls were evaluated by magnetic resonance diffusion-weighted imaging (DW-MRI) and spectroscopy (MRS) at 17.5–18 weeks post-infection, as part of a study of viral clade pathogenesis in FIV-infected cats. The goals of the MR imaging portion of the project were to determine whether this methodology was capable of detecting early neuropathophysiology in the absence of outward manifestation of neurological signs and to compare the MR imaging results for the two viral strains expected to have differing degrees of neurologic effects. We hypothesized that there would be increased diffusion, evidenced by the apparent diffusion coefficient as measured by DW-MRI, and altered metabolite ratios measured by MRS, in the brains of FIV-PPR-infected cats relative to C36-infected cats and uninfected controls. Increased apparent diffusion coefficients were seen in the white matter, gray matter, and basal ganglia of both the PPR and C36-infected (asymptomatic) cats. Thalamic MRS metabolite ratios did not differ between groups. The equivalently increased diffusion by DW-MRI suggests similar indirect neurotoxicity mechanisms for the two viral genotypes. DW-MRI is a sensitive tool to detect neuropathophysiological changes in vivo that could be useful during longitudinal studies of FIV.

Keywords Lentiviral neuropathology · HIV-associated dementia (HAD) · Magnetic resonance spectroscopy (MRS) · Diffusion-weighted imaging (DW-MRI) · Apparent diffusion coefficient (ADC) · FIV-PPR · FIV-C36

D. S. Bucy · A. M. Bachand · M. Morges · S. L. Kraft
Department of Environmental and Radiological Health Sciences, College of Veterinary Medicine and Biomedical Sciences, Colorado State University, Fort Collins, CO, USA

M. S. Brown
Department of Radiology, University of Colorado Health Sciences Center, Aurora, CO, USA

H. Bielefeldt-Ohmann
School of Veterinary Science, University of Queensland, Queensland, Australia

J. Thompson · S. VandeWoude
Department of Microbiology Immunology and Pathology, College of Veterinary Medicine and Biomedical Sciences, Colorado State University, Fort Collins, CO, USA

J. H. Elder
Department of Immunology and Microbial Science, The Scripps Research Institute, La Jolla CA, USA

S. L. Kraft (✉)
James L. Voss Veterinary Teaching Hospital,
300 West Drake Road,
Fort Collins, CO 80523, USA
e-mail: skraft@colostate.edu

Introduction

HIV-associated dementia (HAD) is a poorly understood syndrome of cognitive and motor disorders that occurs in up to 20% of human immunodeficiency virus type I (HIV) infections (McArthur et al. 1993). Direct viral effects, including virus-induced neurotoxicity, and indirect effects, such as cytokine signaling and inflammatory-mediated neuroexcitatory dysfunction, have been implicated (Bell 1998; Dow et al. 1992; Gray et al. 1996). HAD is only partially controlled by current antiretroviral therapies, thus mild forms of the neurologic disease predominate in developed countries (Gray et al. 2003; McArthur et al. 2004). There is also concern that as AIDS patients are living longer with more effective therapies, neurologic disorders will become more common. Sensitive indicators of HAD pathogenesis are needed for early diagnosis, staging, and development of new therapies that better control HAD progression (Pomper and Sacktor 2007).

Animal models are essential to developing a better understanding of lentiviral pathogenesis and for testing effective therapeutics for HAD. Feline immunodeficiency virus (FIV) is a particularly good model for the study of HAD pathogenesis. HIV and FIV are both lentiviruses in the same subfamily that share remarkably similar genetic makeup, structure, and pathogenesis. In addition, FIV is a well-characterized, naturally occurring, reproducible disease considered to have consistent, strain-dependent neuropathogenesis (Meeker 2007; Phillips et al. 2000; Podell et al. 1997, 1993; Power et al. 1998a). The previous studies of FIV have shown it to infect the central nervous system early in infection and cause a neurologic syndrome characterized by specific behavioral abnormalities (Meeker 2007; Phillips et al. 1996; Podell et al. 1993; Steigerwald et al. 1999). Furthermore, the feline model is logistically and economically easier to manage and manipulate in a controlled environment than human clinical studies or non-human primate animal models.

Evidence suggests that viral genotype may play a role in the severity of neuropathogenesis of HIV infection (Bratanich et al. 1998; Power et al. 1998b). As with HIV, FIV subtypes have been characterized that vary in their pathogenesis and neurologic effects (de Rozieres et al. 2004a, 2008; Hein et al. 2003; Power et al. 1998a). FIV-C36 is a highly pathogenic viral clone of the clade C that causes high disease incidence and severity with acute immunodeficiency without documented neurologic effects (de Rozieres et al. 2004a). In contrast, FIV-PPR of the clade A is a strain that has demonstrated neurotropism and virulence, but has less associated systemic pathogenicity than the FIV-C36 isolate (Phipps et al. 2000).

The use of advanced imaging methodology is potentially a sensitive method for the noninvasive longitudinal study of evolving disease processes such as FIV lentiviral neuropathogenesis with the potential for detecting physiological, functional, and metabolic abnormalities prior to clinical manifestation and/or histopathology. There is a need for continued development of preclinical models for testing novel therapeutics for HAD (Crews et al. 2008), and the use of advanced imaging methodology for these animal models could be a powerful adjunct to evaluate preventative or early interventional therapy. Although the use of advanced imaging technology can be relatively expensive and usually requires general anesthesia for animal studies, its noninvasive nature allows the use of fewer animals while reaching meaningful results, thereby sparing cost and optimizing the humane use of animals in preclinical trials.

Magnetic resonance imaging (MRI) has been used to demonstrate the gross anatomic changes associated with late HAD progression, including atrophy of the white matter and basal ganglia (Aylward et al. 1995; Aylward et al. 1993; Ge et al. 2003; Handelsman et al. 1993). MR also has several advanced capabilities that allow the detection of physiologic and metabolic processes, including diffusion-weighted imaging (DW-MRI), diffusion tensor imaging (DTI), and magnetic resonance spectroscopy (MRS). Although DW-MRI and DTI have been used to evaluate HIV patients in a number of human studies, to our knowledge there are few reports on brain diffusion abnormalities in preclinical animal models of HAD (He et al. 2003). Furthermore, the understanding of metabolic abnormalities as determined by MRS in preclinical models remains limited to only a few time points (Cloak et al. 2004b; Fuller et al. 2004; Gonzalez et al. 2006; Greco et al. 2002, 2004; Lentz et al. 2008a, b; Podell et al. 1999; Power et al. 1998a; Ratai et al. 2009). We performed MRI to investigate its usefulness for this application, at a single 4-month post-inoculation (PI) time point on a subset of FIV-infected cats from an ongoing study of viral clade pathogenesis (de Rozieres et al. 2008). The goals of the MRI portion of the project were to determine whether clinical MRI methodology was capable of detecting early neuropathophysiology in these cats prior to outward manifestation of neurological signs and to compare MR imaging results for two viral strains expected to have differing degrees of neurologic effects. The MRI results were evaluated in light of evidence for systemic pathogenicity including plasma viremia and proviral loads and degree of immunodeficiency. We anticipated that physiological methods of MRI such as DW-MRI or MRS would be more sensitive than anatomic MR imaging to neurological abnormalities in these cats. We hypothesized that there would be increased diffusion measured by DW-MRI measured as the apparent diffusion coefficient (ADC), and altered metabolite ratios measured by MRS in the brains of FIV-PPR-infected cats, relative to C36-infected cats and

uninfected controls. These data would provide preliminary evidence for the role of viral genotype on neurological effects of FIV.

Results

All cats remained clinically and neurologically normal throughout the study and had no visible gross lesions on the anatomic MR and the DW-MRI images. No clinical signs were observed in these cats other than mild lymphadenopathy and gingivitis. No treatments were instituted relative to FIV-induced disease. The ADCs derived from the DW-MRI of the FIV-PPR and FIV-C36-infected cat brains were significantly greater than the mean corresponding values from the control cats for the white matter, gray matter, and basal ganglia. The increase in ADC values, therefore diffusion, was small at approximately 3–6% (Fig. 1). The ADC values did not differ between infected cat brains and the control cats for the other brain regions including midbrain, brainstem, and cerebellum. The ADCs of the infected cats were equivalently increased and did not statistically differ between the two viral clades, FIV-PPR and FIV-C36, for any brain region. For all cat groups, the ADC values differed consistently by brain region, being generally highest in the gray matter. The magnitude of ADC values decreased slightly with increasing b factor for all tissues.

Data reproducibility was assessed by scanning control cats twice, and paired t tests showed no significant differences between the ADC values of the two scans for any brain region (data not shown). For b factors of 1,000 and 1,500, the coefficient of variation (CV) for ADC fell between 1% and 6% for five of the eight brain regions and was 8% for the basal ganglia and 9% for the brainstem. For b factor of 2,000, the coefficient of variation was less than 5% for seven of the eight brain regions. A considerably greater coefficient of variation was found for the cerebellum at all b factors and ranged from 15% to 22%. For most analyses, the ADC values from the two scans were averaged for each brain region including the cerebellum for consistency. However, for the cerebellum, the analyses were repeated using scan 1 ADC values only due to its high variability.

The N-acetyl-aspartate (NAA)/creatine (Cr) and choline (Cho)/Cr ratios derived from MR spectroscopy of the thalamus did not differ from control groups (Table 1).

Plasma viremia and proviral load for FIV-C36 cats were approximately two orders of magnitude greater than FIV-PPR-infected cats throughout the course of the infection. Plasma viremia for the FIV-PPR-infected cats peaked at 7.57×10^4 RNA copies/ml peripheral blood at 10 days post-inoculation and FIV-C36-infected cats peaked at 6.17×10^7 RNA copies/ml peripheral blood at 14 days post-inoculation (Fig. 2a; de Rozieres et al. 2008). Proviral load peaked at day 35 for both FIV-PPR and FIV-C36-infected cats with values of 3.47×10^3 and 1.35×10^5 per 10^6 peripheral blood mononuclear cells, respectively (Fig. 2b; de Rozieres et al. 2008).

The CD4/CD8 lymphocyte ratios increased initially, 7–14 days post-inoculation, and then declined throughout the remainder of the study for all groups, including controls (de Rozieres et al. 2008). The CD4/CD8 ratios for FIV-PPR-infected cats and controls did not differ, with values of approximately 1.5 at the time of MR imaging. The FIV-C36-infected cats had significantly decreased CD4/CD8 ratios in the later time points (>100 days PI) compared to controls, with values near 1.0 at the time of the MR imaging (111–127 days PI; Fig. 2c).

At the end of study (6 months PI) proviral loads in the brainstem, globus pallidus and putamen, caudate nucleus, and cortex varied by brain region and were greater in the FIV-C36 infected cats than FIV-PPR-infected cats in all sections. FIV-PPR proviral loads were below detection limits (ten copies per million cell equivalents) in more than half of the tissues assayed (Fig. 3). The significantly lower level of provirus in FIV-PPR-infected cats is similar to findings in peripheral cells (Fig. 2b).

Histopathology revealed only mild changes in the brains of infected cats. Most FIV-PPR and FIV-C36-infected cats had

Fig. 1 Apparent diffusion coefficients across multiple brain regions in cats infected with FIV-PPR, FIV-C36, and age-matched controls with b factor= 2,000. *Error bars* represent one standard deviation of the mean (*$p<0.05$, Tukey's test)
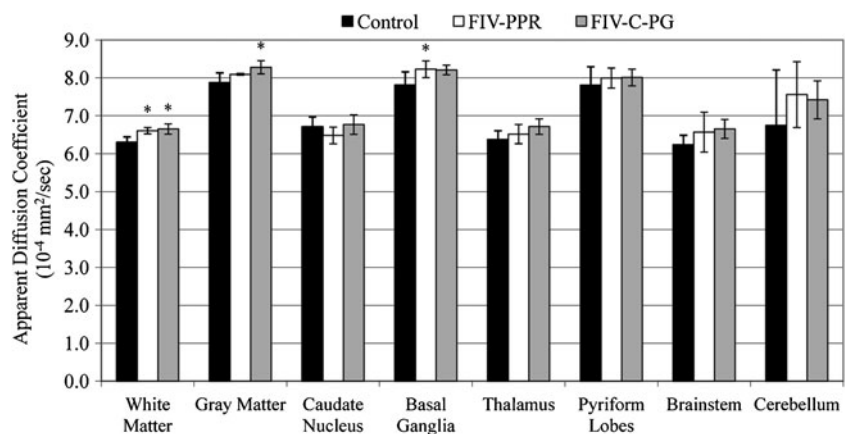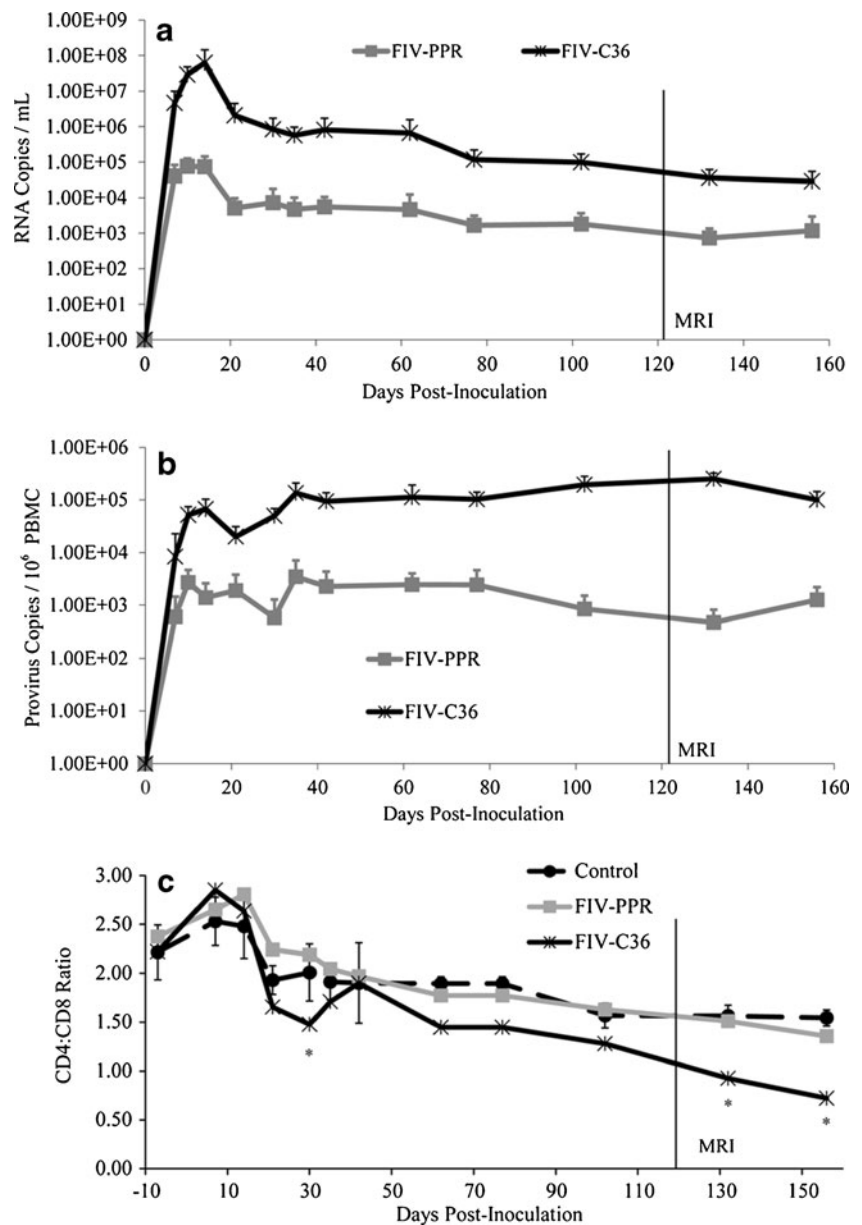
Table 1 Average metabolite ratios from the thalamus of FIV-infected cats and age-matched controls

	NAA/Cr	SD	p value	Cho/Cr	SD	p value
Control	1.60	0.19	–	2.65	0.17	–
FIV-PPR	1.43	0.17	0.38	2.53	0.35	0.95
FIV-C36	1.56	0.03	0.93	2.71	0.64	0.99

NAA/Cr and Cho/Cr metabolite ratios measured with multivoxel MR spectroscopy of the thalamus of infected cats and controls. p values are the results of Tukey's tests for pair wise comparisons between FIV-infected groups and controls. No significant differences were seen groups for either NAA/Cr or Cho/Cr

SD standard deviation

equivalent minimal to mild dispersed or more vasculocentric infiltration of lymphocytes, plasma cells, and monocyte/ macrophages in the meninges and in the arachnoid of small penetrating vessels. In addition, in two of the FIV-PPR-infected cats, there was mild microgliosis and multifocal neuron degeneration with satellitosis in the basal ganglia and caudate nucleus. Many of the infiltrating leukocytes, most notably in the meninges, displayed signs of activation, including upregulated expression of phospho-p38α-MAPK (Fig. 4).

Discussion

The first of our two objectives for this initial investigation in FIV-infected cats was to determine whether anatomical or

Fig. 2 Plasma viremia (*a*), proviral load (*b*), and CD4/CD8 lymphocyte ratios (*c*) in FIV-PPR and FIV-C36-infected cats. Control cats had undetectable plasma viremia (data not shown). *Error bars* represent one standard deviation of the mean. MRI imaging and spectroscopy, indicated by a *vertical line*, was performed between 111 and 127 days PI for all cats. These data demonstrate the context of the timing of the MR studies (de Rozieres et al. 2008). For ease of viewing the CD4/ CD8 lymphocyte ratios, *error bars* (standard deviation) are shown for the control group only. Statistically significant values (*p*<0.05) relative to controls are signified by *asterisks*
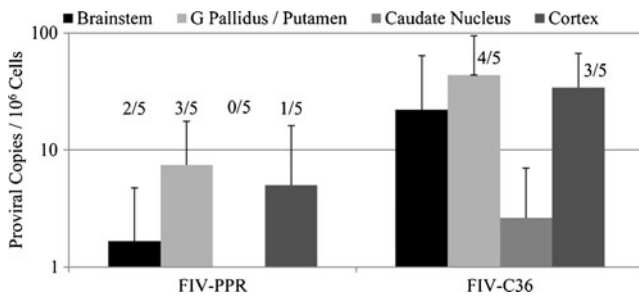
Fig. 3 Brain proviral load at 6 months PI in FIV-PPR and FIV-C36-infected cats. Each sample from each individual animal was run in triplicate and average viral loads calculated. FIV-C36-infected cats had higher proviral loads than PPR-infected cats in all regions, and provirus was undetectable in the majority of samples from FIV-PPR animals. *Fraction above each bar* indicates fraction of animals with detectable provirus. Five of the five samples were positive in animals where a fraction is not indicated

physiological indicators of neuropathology could be detected by MRI. No anatomical gross lesions were observed with routine MR imaging, which was not unexpected at this early PI time period. However, increased brain diffusion was detected in multiple brain regions using DW-MRI, at 17.5–18 weeks PI in these asymptomatic cats. The increased diffusion in these infected cat brains was of similar magnitude and in similar brain regions as in a previous report on HIV patients with mild dementia (Cloak et al. 2004a; Usiskin et al. 2007; Yoon et al. 2007). This illustrates the highly sensitive ability of DW-MRI to detect small fluid shifts from neuropathophysiology not yet sufficient to cause visible signal nor anatomic changes on conventional MR images. These findings are in agreement with the previously proposed mechanism of neuronal injury during HIV and FIV infection due to indirect effects from cytokines, chemokines, and glutamate released by activated leukocytes and microglial cells (Bell 1998; Eggert et al. 2009; Gray et al. 1996; Meeker 2007; Poli et al. 1999).

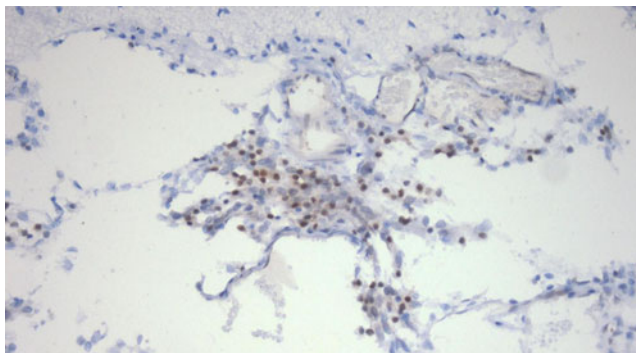DW-MRI and DTI detect physiological changes in the random motion of water molecules, or diffusion. Altered

Fig. 4 Photomicrograph of the meninges of an FIV-infected cat with infiltrating lymphocytes. The lymphocytes expressed phospho-p38 MAPK, indicating activation

diffusion can be semi-quantified using DW-MRI as the apparent diffusion coefficient, or ADC, which in inflammatory processes is thought to be secondary to the breakdown of barriers to the flow of water during microscopic brain injury (Gass et al. 2001; Le Bihan et al. 1986). Tissue changes can be detected by ADC quantification during region of interest analysis even when signal changes on diffusion images are imperceptible and can provide better characterization of infectious brain processes (Mascalchi et al. 2005). Increased frontal white matter diffusion has been demonstrated in the brains of HIV-infected patients using DW-MRI, reflecting inflammation and cellular injury (Cloak et al. 2004a; Usiskin et al. 2007; Yoon et al. 2007). DW-MRI is performed by applying a series of MR diffusion gradients during imaging, allowing the random movement of free water to be semi-quantified. The degree of diffusion weighting, expressed as the *b* factor, is based on the strength and timing of the diffusion gradients; the greater the degree of diffusion weighting, the greater the *b* factor (Cercignani and Horsfield 2001). Certain tissues such as cerebral white matter have fiber bundles with non-random orientation and diffusion of fluid in this tissue is anisotropic in nature. DTI would be preferable for detecting diffusion differences because it accounts for directional water diffusion which is particularly important for white matter fiber tracts, but it was not available on our MRI equipment for this study (Filippi et al. 2001; Pomara et al. 2001; Ragin et al. 2005; Stebbins et al. 2007). DTI has sensitively detected altered diffusion and fractional anisotropy in a variety of scenarios with HIV patients (Chang et al. 2008; Chen et al. 2009; Filippi et al. 2001; Gongvatana et al. 2009; Muller-Oehring et al. 2010; Pfefferbaum et al. 2009; Pomara et al. 2001; Ragin et al. 2004, 2005; Stebbins et al. 2007; Wu et al. 2006).

The optimal DW-MRI *b* factor varies by disease process, species, and tissue type and was unknown for this application so we performed DW-MRI using three different *b* factors. Although differences were seen with all *b* values, overall the *b* factor of 2,000 most consistently showed significant ADC differences and was most reliable when two scans were performed on control cats. The ADC values decreased with increasing *b* factor which was unexpected because theoretically, diffusion sensitivity should go up with higher *b* factor. This has been found with other studies evaluating a range of *b* values and is likely related to the complex biexponential nature of the diffusion decay process which transitions over a range of *b* values because of shifts in dominance of rapid extracellular and slower intracellular diffusion components (DeLano et al. 2000). The development of an advanced mathematical model to estimate diffusion decay in FIV-infected cat brains was not in the scope of this initial study but could be considered in the future by designing more intensive DW-MRI experiments.

Although DW-MRI was capable of detecting early neuropathogenesis in FIV cats, the relatively small size of the feline brain led to sampling challenges due to the proximity to the frontal bone and large frontal sinuses, the osseous tentorium, and large tympanic bullae. The resulting susceptibility artifact and distortion near those structures limited the region of interest (ROI) sampling locations on the ADC maps for the feline frontal and cerebellar regions and led to increased sampling variability particularly for the cerebellum (Fig. 1). Also, for this study we used a 1.5 T MRI instrument and DW-MRI and MRS pulse sequences that are typical of clinical examinations. This provided a realistic picture of achievable results in a translational clinical setting. However, the inherent signal-to-noise obtained from this scenario is lower than might be obtained using a high field strength MRI unit such as that which might be found in an experimental laboratory animal setting. The higher signal-to-noise associated with a higher field MR instrument would have improved the diffusion and spectroscopic measurements. Finally, another limitation of our study is that the number of animals studied was small, which affected the power of our statistical analyses. However, our small sample size was similar to that of comparable studies and despite the low number of subjects, statistical differences were detected.

MRS is another MR technique potentially capable of detecting brain abnormalities prior to neurological signs in HIV infection. Metabolic alterations have been found in HIV-1 patients including increased myoinositol (MI)/Cr ratios, increased Cr, and decreased NAA indicating glial injury and inflammation, and neuronal injury or loss, respectively, in HIV-1 patients exhibiting dementia. These alterations have been mild or minimal in asymptomatic patients and severe in patients with dementia or other neurological impairment (Barker et al. 1995; Chang et al. 2002, 2003, 2004; Chong et al. 1993; Cloak et al. 2004a; Laubenberger et al. 1996; Marcus et al. 1998; Sacktor et al. 2005; Tarasow et al. 2003; Wenserski et al. 2003; Wilkinson et al. 1997). MRS abnormalities in preclinical animal models have been used to infer underlying mechanisms of HAD, to predict its eventual development, and to evaluate various drug treatments. Decreased NAA/Cr ratios have been found in FIV-infected cats within the frontal white matter in vivo and also ex vivo by high resolution nuclear magnetic resonance 12 months PI, but not at 6 months PI (Podell et al. 1999). In macaques with SIV infection, transient decreases in NAA/Cr and increased MI/Cr and Cho/Cr have been shown to occur acutely at the time of peak viremia at 2 weeks PI (Greco et al. 2004; Ratai et al. 2009; Williams et al. 2005). Elevated basal ganglia Cho/Cr found at 4 weeks PI have preceded eventual development of SIV encephalitis (Fuller et al. 2004). Other studies using the macaque SIV model have shown that the acute transient decrease in NAA/Cr is correlated with decreased synaptic integrity rather than neuronal loss (Lentz et al. 2005; Williams et al. 2005). MRS of macaques with an accelerated form of SIV infection has recently been shown to be a good indicator of effective neuroprotection by therapy with minocycline or CNS improvement from combination antiretroviral therapy (Ratai et al. 2010; Williams et al. 2005).

In our study, MRS did not detect significant changes in metabolite ratios at 4 months PI time. This may have been related to the 4-month PI timing since metabolic changes can be normalized during this time period after the acute viremic phase. Also, sampling location may have played a role because we sampled the thalamus (rather than frontal lobes) to avoid the frontal sinuses which had associated magnetic inhomogeneity. Although NAA/Cho ratios were decreased in the thalamus of neurologically affected HIV positive individuals (Meyerhoff et al. 1996), more consistent spectral abnormalities have since been reported for frontal white matter, deep white matter, and basal ganglia locations. The relatively long TE in our MRS protocol was used to optimize detection of NAA and Cr, but was inaccurate for MI and would have prevented our detection of altered MI ratios. An additional limitation is that these data were measured as metabolite ratios based on creatine as a reference standard, rather than as absolute concentrations. The use of ratios could prevent detection of absolute changes in creatine concentration, assuming that NAA or choline concentrations had also changed.

Our second goal was to compare MR imaging results for two viral strains that reportedly have differing degrees of neurologic effects. Our initial hypothesis of viral strain-dependent neuropathophysiology by DW-MRI was not supported since nearly equivalent increases in diffusion were seen in both FIV-PPR and FIV-C36-infected cats. This may reflect a relatively low threshold effect from indirect cytokine effects, regardless of degree of viremia or proviral loads, systemic pathogenicity, or viral strain. The MRI results obtained at 17.5–18 weeks PI may reflect the initial phase of CNS inflammation.

Although longitudinal assessment of ADC and a direct comparison with histopathology would have been useful, this was not possible because the MRI examinations were added to an existing viral pathogenesis FIV project with a predetermined timeline. Only a single time point for MRI was possible, and there was an unavoidable significant 33–37-day time interval between the MRI scans and necropsy. A future longitudinal study would be needed with serial MRIs and direct histopathological correlation to determine the exact nature and correspondence of the temporal changes through the acute and chronic PI time periods.

It is interesting to note, however, that at the time point of euthanasia, only minimal histological differences were seen

between the two viral strains in the degree of brain inflammatory cell infiltration. The cats infected with FIV-C36 had low but detectable brain provirus which is likely a reflection of the higher plasma proviral and viremic levels for the cats infected with that viral strain. In comparison, the very low proviral and viral loads in FIV-PPR-infected animals are likely due to both viral inoculum and host immune characteristics. Although FIV-C36 infection has been shown to cause acute immunodeficiency without documented neurologic effects, in this study these cats had similar diffusion changes during the inflammatory phase and similar brain histopathology as the FIV-PPR cats, suggesting comparable degree of neurotoxicity effects at those time periods. Therefore, it remains possible that cats with FIV-C36 have lacked clinical neurological problems because they succumb to their disease before neurological signs typically begin, which is at the 14–15-week time period for FIV-PPR-infected cats (de Rozieres et al. 2004a, b, 2008; Hokanson et al. 2000; Phillips et al. 1996). The low level of viral infection detected in brain tissues in this study would also suggest that neuropathogenicity is not directly related to viral load or active viral replication. This implies that early antiretroviral therapy to decrease viral loads in the CNS are only likely to have a demonstrable effect on HAD development if CNS viral load is proportionate to viral load in the periphery.

In conclusion, DW-MRI detected increased brain diffusion at 17.5–18 weeks PI in neurologically asymptomatic cats with FIV infection from two different viral clades with historically reported differences in neurological manifestation. Both viral strains led to similarly increased brain diffusion despite differences in peripheral viremia and proviral load, implicating indirect threshold-associated effects from secondary cytokines. Advanced MR imaging techniques, such as DW-MRI, DTI, and MRS, have a promising role in furthering our understanding of the mechanisms of pathogenesis of HAD and for preclinical testing of new therapies.

Methods

Animals and inoculation

Fifteen 14–16-week-old specific pathogen-free (SPF) cats obtained from Cedar River Laboratories, Ames IA, and an SPF cat colony at Colorado State University, Fort Collins, CO were kept in barrier rooms in facilities accredited by AAALAC International. All procedures were approved by the CSU Institutional Animal Care and Use Committee following standards established in the *Guide for the Care and Use of Laboratory Animals* (National Academy of Science, National Academy Press, Washington D.C.). The cats were randomized by age and sex, and each cat was inoculated both orally (0.5 ml) and intravenously (0.5 ml) with $10^{3.5}$ $TCID_{50}$ particles/ml of either FIV-PPR ($n=5$) or FIV-C36 ($n=5$) as described previously (de Rozieres et al. 2008). Uninfected controls ($n=5$) were administered only media. Animals were examined daily for evidence of clinical disease, and physical exams were performed during blood collections. Blood samples were collected at days −7, 7, 10, 14, 21, 30, 35, 42, 62, 77, 102, 132, and 156 PI on un-anesthetized animals. Samples were collected and measured for CD4+ and CD8+ lymphocytes, proviral DNA and plasma RNA as described previously (de Rozieres et al. 2008).

MRI, DW-MRI, and MRS

MRI was done with a General Electric Signa LX 1.5 T MR HiSpeed Plus System (Milwaukee, USA). Imaging was performed with cats under general anesthesia maintained with isoflurane gas via a non-rebreathing circuit and positive pressure ventilation. Each of the FIV-infected cats was scanned once between 123 and 127 days (17.5–18 weeks) post-inoculation. All five control cats also underwent MRI scans. Four of the five control cats were scanned twice in order to assess baseline variability; the double control animal scans took place within a 3–5-day time period, between 111 and 127 days post-sham inoculation. Cats were positioned in sternal recumbency with the head placed on foam sponges to center it within the quadrature head coil, using the three plane localizer series to verify location of the pituitary fossa in the center of the coil and laser light localization to standardize consistent longitudinal orientation along the z axis. Animals were in a deep plane of general anesthesia with their heads well-secured in the imaging coil, therefore there was no head movement during image acquisition. A complete anatomic brain MRI scan was performed using multiple pulse sequences. These included transverse dual fast spin echo proton density/T2-weighted scan (TR=4,000 ms, TE=17/115 ms, echo train length=16, slice thickness=3 mm, image matrix=256×256), FLAIR (TR=8125 ms, TE=120 ms, TI=2,200 ms), and transverse T1-weighted scans (TR=550 ms, TE = minimal) before and post-contrast T1 transverse, dorsal, and sagittal images after intravenous gadolinium DTPA, Magnevist, at 0.5 mmol/kg (Bayer Pharmaceuticals, Wayne, NJ). Diffusion-weighted imaging was performed at b factors of $b=1,000$, $b=1,500$, and $b=2,000$ using TE=90–110 ms, TR=8,000 ms, FOV=24 mm, slice thickness=5 mm, image matrix=124×124, using NEX of 1, 2, or 4 (respectively for the three different b factors) in order to determine the most appropriate b factor value for this application. Multivoxel proton MRS centered at the level of the thalamus was acquired using the point-resolved spectroscopy sequence, with a TR=1,500 ms, TE=135 ms,
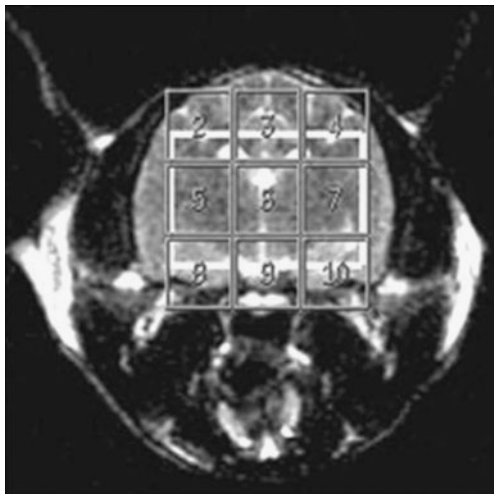
Fig. 5 Transverse T2-weighted MR feline brain image showing placement of the excitation voxel (*white rectangle*) and the overlaid multivoxel phase encoding grid (in *gray*). Voxels 5–7 correspond to the feline thalamus

field of view 16 cm, and slice thickness=10 mm, 256 averages (Fig. 5).

Euthanasia, histology, and brain proviral load

Full necropsies were performed at 160–161 days PI. This represented a time interval between MRI and necropsy of 43–49 days for control cats, and 33–37 days for FIV-infected cats. Euthanasia was performed with an overdose of pentobarbital while cats were under ketamine and acepromazine sedation, then tissues were examined, collected, and either fixed in 10% neutral-buffered formaldehyde or snap-frozen for later RNA- and DNA-isolation. Samples from brain (left cerebral hemisphere, left sides of the cerebellum and brainstem), lymphoid tissues (thymus,

spleen, tonsil, submandibular lymph node, several mesenteric lymph nodes, prescapular, and popliteal lymph nodes), and gastrointestinal tract (jejunum, ileum with Peyer's patch, and colon) were fixed for 72 h, followed by storage in 70% ethanol until routine processing for paraffin embedding. Five-micrometer tissue sections were stained with hematoxylin and eosin (H&E) and examined on an Olympus BX41 microscope equipped with a Q-Color3 camera (Olympus) and corresponding computer software. Brain proviral load determinations were made by polymerase chain reaction (PCR) from the brainstem, globus pallidus and putamen, caudate nucleus, and cerebral cortex.

Viral RNA was extracted from plasma collected from EDTA-treated whole blood following centrifugation. Plasma was frozen at −70°C until processing. RNA was purified from 140 μl of plasma using a QIAamp Viral RNA Mini Kit (Qiagen, Valencia, CA). SuperscriptII (Invitrogen, Carlsbad, CA) was implemented in reactions with random hexamers (Invitrogen) added and treated with RNase Out (Invitrogen) for preparation of cDNA from viral RNA. Genomic DNA was extracted from peripheral blood mononuclear cells purified on a Histopaque-1077 (Sigma, St. Louis, MO) gradient. Cells were washed and pellets frozen at −20°C overnight. DNA was isolated using a DNeasy Tissue Kit (Qiagen, Valencia, CA). Real-time PCR was performed on an iCycler thermocycler (Bio-Rad, Hercules, CA) to detect both proviral DNA and plasma viremia using the AmpliTaq Gold DNA polymerase-containing TaqMan Universal PCR Master Mix (Applied Biosystems, Foster City, CA). Derivation of FIV-A and FIV-C primer/probe sets and sequences have been previously described (Pedersen et al. 2001). PCR reactions in a total volume of 25 μl consisted of 12.5 μl master mix, 0.5 μl each of 20 μM forward and reverse primers, 0.2 μl of 10 μM probe, and 5 μl template. After 2 min at 50°C, the

Fig. 6 Transverse proton density MR feline brain images illustrating the locations of the ROI's used for the analysis; images such as these were used to locate anatomic structures and their coordinates were used to accurately place the ROI's on the ADC maps generated from diffusion images (*w* = white matter, *g* = gray matter, *cn* = caudate nucleus, * = approximate region of putamen and globus pallidus, *T* = thalamus, *P* = pyriform lobe, *B* = brainstem/midbrain, *C* = cerebellum)
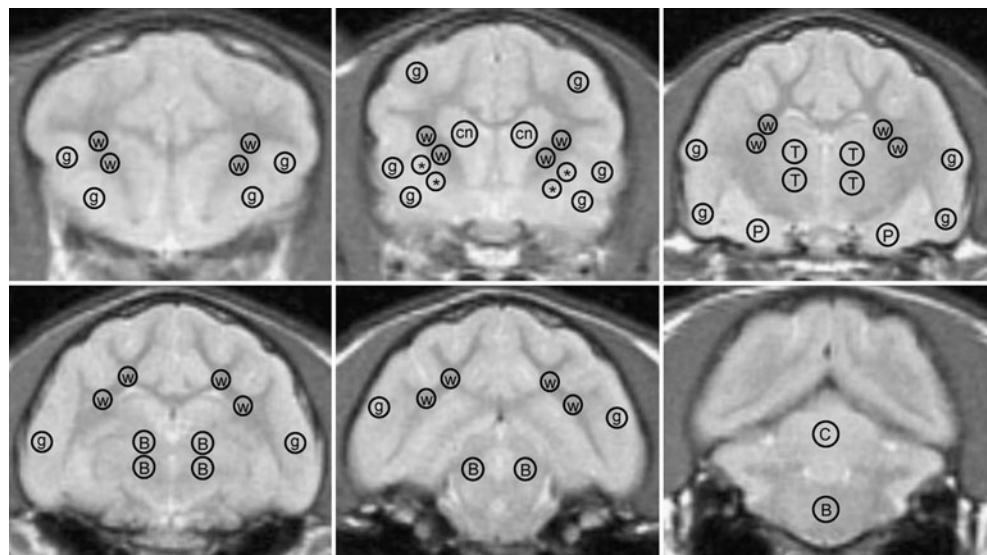
AmpliTaq Gold DNA polymerase was activated at 95°C for 10 min, followed by 45 cycles of 95°C for 15 s and 60°C for 1 min. Threshold cycle values (CT) were defined as the point at which the fluorescence passed a threshold limit. The calculation of copy number for FIV provirus was done using a standard curve generated from dilutions of a sub-cloned *gag* PCR product. To calculate copy number of viral RNA in plasma, a standard curve was generated by diluting FIV-PPR virus stock in naïve cat plasma, preparing cDNA as described above, and comparing CT values to those of the sub-cloned *gag* standard.

To characterize inflammatory reactions in the brain, immunohistochemistry was carried out as described previously in detail (Bielefeldt-Ohmann et al. 2008; Tolnay et al. 2010). Briefly, paraffin sections collected on charged slides were deparaffinized, subjected to antigen-retrieval and blocking steps, and then incubated with primary antibodies specific for hemeoxygenase-1, inducible nitric oxide synthase, vascular endothelial growth factor-A, phospho-p38α MAPK, and the apoptosis marker activated caspase-3. Additional sections were also labeled for glial fibrillary acidic protein to assess for gliosis or loss of astrocytes, for microglial cells using the Iba-1 marker, and for oligodendrocytes using the transcription factor OLIG2 as cell marker. All H&E and immunolabeled sections were examined by a single veterinary pathologist (HBO) blinded to the grouping of the animals.

Blood was processed on the days noted above and CD4/CD8 lymphocyte ratios were calculated using standard flow cytometric analysis as reported. Proviral DNA and plasma RNA calculation and statistical analysis were also performed as described previously (de Rozieres et al. 2008).

DW-MRI and MRS data analysis

All pulse sequences from the MRI examinations were reviewed by a single veterinary radiologist (SLK) for gross lesions. Diffusion-weighted images were first assessed subjectively, and ADC maps were then generated using ROI analysis using commercial software (Functool, General Electric Medical Systems, Milwaukee, WI). A total of 58 standardized ROIs were placed by a single research assistant (DSB), and all ROIs were verified by the radiologist (SLK) on the ADC maps on specific areas throughout each cat brain (Fig. 6). The higher image quality proton density images were used to first locate ROI's at specific anatomic locations (Fig. 6). The *x*, *y* coordinates of those ROIs were noted from the proton density images, and then those same image coordinates were used to place identically sized ROIs on the ADC maps in order to sample the same brain anatomy. Areas of interest included multiple white and gray matter points, the region of the basal ganglia (including the areas of the caudate nuclei, globus pallidus, and putamen), thalamus, pyriform lobes, midbrain/brain-

stem, and cerebellum. Data were collected and grouped and averaged by brain region for each treatment group.

Reproducibility of the DWI-MR scans was assessed by conducting two scans on the control cats, which was possible for only four of the five cats. We conducted paired *t* tests and calculated the CV for each brain region (between-trial variability relative to the mean; Hopkins 2000).

To test for differences in ADC values between brain regions and between groups (control, FIV-PPR, and FIV-C36) and to determine if differences between groups depended on the brain region we used repeated measures analysis of variance. Pair wise comparisons between groups were conducted using Tukey's test (which corrects for multiple comparisons). Assumptions for all statistical methods were tested and found to hold.

Magnetic resonance (^{1}H) proton spectra were analyzed offline by a single MR physicist (MSB) using LC Model software (Stephen Provencher Inc., Oakville, Ontario, Canada) to derive ratios of Cho and NAA to Cr as an internal reference, for those voxels of the multivoxel complex that were centered within the thalamus. NAA/Cr and Cho/Cr ratios were then averaged and analyzed with Tukey's tests for pair wise comparisons between FIV-PPR and FIV-C36-infected cats and controls.

References

Aylward EH, Henderer JD, McArthur JC, Brettschneider PD, Harris GJ, Barta PE, Pearlson GD (1993) Reduced basal ganglia volume in HIV-1-associated dementia: results from quantitative neuro-imaging. Neurology 43:2099–2104

Aylward EH, Brettschneider PD, McArthur JC, Harris GJ, Schlaepfer TE, Henderer JD, Barta PE, Tien AY, Pearlson GD (1995) Magnetic resonance imaging measurement of gray matter volume reductions in HIV dementia. Am J Psychiatry 152:987–994

Barker PB, Lee RR, McArthur JC (1995) AIDS dementia complex: evaluation with proton MR spectroscopic imaging. Radiology 195:58–64

Bell JE (1998) The neuropathology of adult HIV infection. Rev Neurol (Paris) 154:816–829

Bielefeldt-Ohmann H, Tolnay AE, Reisenhauer CE, Hansen TR, Smirnova N, Van Campen H (2008) Transplacental infection with non-cytopathic bovine viral diarrhoea virus types 1b and 2: viral spread and molecular neuropathology. J Comp Pathol 138:72–85

Bratanich AC, Liu C, McArthur JC, Fudyk T, Glass JD, Mittoo S, Klassen GA, Power C (1998) Brain-derived HIV-1 tat sequences from AIDS patients with dementia show increased molecular heterogeneity. J Neurovirol 4:387–393

Cercignani M, Horsfield MA (2001) The physical basis of diffusion-weighted MRI. J Neurol Sci 186(Suppl 1):S11–S14

Chang L, Ernst T, Witt MD, Ames N, Gaiefsky M, Miller E (2002) Relationships among brain metabolites, cognitive function, and viral loads in antiretroviral-naive HIV patients. Neuroimage 17:1638–1648

Chang L, Ernst T, Witt MD, Ames N, Walot I, Jovicich J, DeSilva M, Trivedi N, Speck O, Miller EN (2003) Persistent brain abnormalities in antiretroviral-naive HIV patients 3 months after HAART. Antivir Ther 8:17–26

Chang L, Lee PL, Yiannoutsos CT, Ernst T, Marra CM, Richards T, Kolson D, Schifitto G, Jarvik JG, Miller EN, Lenkinski R, Gonzalez G, Navia BA (2004) A multicenter in vivo proton-MRS study of HIV-associated dementia and its relationship to age. Neuroimage 23:1336–1347

Chang LD, Wong V, Nakama H, Watters M, Ramones D, Miller EN, Cloak C, Ernst T (2008) Greater than age-related changes in brain diffusion of HIV patients after 1 year. J Neuroimmune Pharmacol 3:265–274

Chen Y, An H, Zhu H, Stone T, Smith JK, Hall C, Bullitt E, Shen D, Lin W (2009) White matter abnormalities revealed by diffusion tensor imaging in non-demented and demented HIV+ patients. Neuroimage 47:1154–1162

Chong WK, Sweeney B, Wilkinson ID, Paley M, Hall-Craggs MA, Kendall BE, Shepard JK, Beecham M, Miller RF, Weller IV et al (1993) Proton spectroscopy of the brain in HIV infection: correlation with clinical, immunologic, and MR imaging findings. Radiology 188:119–124

Cloak CC, Chang L, Ernst T (2004a) Increased frontal white matter diffusion is associated with glial metabolites and psychomotor slowing in HIV. J Neuroimmunol 157:147–152

Cloak CC, Chang L, Ernst T, Barr MC, Huitron-Resendiz S, Sanchez-Alavez M, Phillips TR, Henriksen S (2004b) Methamphetamine and AIDS: 1HMRS studies in a feline model of human disease. J Neuroimmunol 147:16–20

Crews L, Lentz MR, Gonzalez RG, Fox HS, Masliah E (2008) Neuronal injury in simian immunodeficiency virus and other animal models of neuroAIDS. J Neurovirol 14:327–339

de Rozieres S, Mathiason CK, Rolston MR, Chatterji U, Hoover EA, Elder JH (2004a) Characterization of a highly pathogenic molecular clone of feline immunodeficiency virus clade C. J Virol 78:8971–8982

de Rozieres S, Swan CH, Sheeter DA, Clingerman KJ, Lin YC, Huitron-Resendiz S, Henriksen S, Torbett BE, Elder JH (2004b) Assessment of FIV-C infection of cats as a function of treatment with the protease inhibitor, TL-3. Retrovirology 1:38

de Rozieres S, Thompson J, Sundstrom M, Gruber J, Stump DS, de Parseval AP, VandeWoude S, Elder JH (2008) Replication properties of clade A/C chimeric feline immunodeficiency viruses and evaluation of infection kinetics in the domestic cat. J Virol 82:7953–7963

DeLano MC, Cooper TG, Siebert JE, Potchen MJ, Kuppusamy K (2000) High-b-value diffusion-weighted MR imaging of adult brain: image contrast and apparent diffusion coefficient map features. AJNR Am J Neuroradiol 21:1830–1836

Dow SW, Dreitz MJ, Hoover EA (1992) Feline immunodeficiency virus neurotropism: evidence that astrocytes and microglia are the primary target cells. Vet Immunol Immunopathol 35:23–35

Eggert D, Dash PK, Serradji N, Dong CZ, Clayette P, Heymans F, Dou H, Gorantla S, Gelbard HA, Poluektova L, Gendelman HE (2009) Development of a platelet-activating factor antagonist for HIV-1 associated neurocognitive disorders. J Neuroimmunol 213:47–59

Filippi CG, Ulug AM, Ryan E, Ferrando SJ, van Gorp W (2001) Diffusion tensor imaging of patients with HIV and normal-appearing white matter on MR images of the brain. American Journal of Neuroradiology 22:277–283

Fuller RA, Westmoreland SV, Ratai E, Greco JB, Kim JP, Lentz MR, He J, Sehgal PK, Masliah E, Halpern E, Lackner AA, Gonzalez RG (2004) A prospective longitudinal in vivo 1H MR spectroscopy study of the SIV/macaque model of neuroAIDS. BMC Neurosci 5:10

Gass A, Niendorf T, Hirsch JG (2001) Acute and chronic changes of the apparent diffusion coefficient in neurological disorders—biophysical mechanisms and possible underlying histopathology. J Neurol Sci 186(Suppl 1):S15–S23

Ge Y, Kolson DL, Babb JS, Mannon LJ, Grossman RI (2003) Whole brain imaging of HIV-infected patients: quantitative analysis of magnetization transfer ratio histogram and fractional brain volume. AJNR Am J Neuroradiol 24:82–87

Gongvatana A, Schweinsburg BC, Taylor MJ, Theilmann RJ, Letendre SL, Alhassoon OM, Jacobus J, Woods SP, Jernigan TL, Ellis RJ, Frank L, Grant I (2009) White matter tract injury and cognitive impairment in human immunodeficiency virus-infected individuals. J Neurovirol 15:187–195

Gonzalez RG, Greco JB, He J, Lentz MR, O'Neil S, Pilkenton SJ, Ratai EM, Westmoreland S (2006) New insights into the neuroimmunity of SIV infection by magnetic resonance spectroscopy. J Neuroimmune Pharmacol 1:152–159

Gray F, Scaravilli F, Everall I, Chretien F, An S, Boche D, Adle-Biassette H, Wingertsmann L, Durigon M, Hurtrel B, Chiodi F, Bell J, Lantos P (1996) Neuropathology of early HIV-1 infection. Brain Pathol 6:1–15

Gray F, Chretien F, Vallat-Decouvelaere AV, Scaravilli F (2003) The changing pattern of HIV neuropathology in the HAART era. J Neuropathol Exp Neurol 62:429–440

Greco JB, Sakaie KE, Aminipour S, Lee PL, Chang LL, He J, Westmoreland S, Lackner AA, Gonzalez RG (2002) Magnetic resonance spectroscopy: an in vivo tool for monitoring cerebral injury in SIV-infected macaques. J Med Primatol 31:228–236

Greco JB, Westmoreland SV, Ratai EM, Lentz MR, Sakaie K, He J, Sehgal PK, Masliah E, Lackner AA, Gonzalez RG (2004) In vivo 1H MRS of brain injury and repair during acute SIV infection in the macaque model of neuroAIDS. Magn Reson Med 51:1108–1114

Handelsman L, Song IS, Losonczy M, Park S, Jacobson J, Wiener J, Aronson M (1993) Magnetic resonance abnormalities in HIV infection: a study in the drug-user risk group. Psychiatry Res 47:175–186

He J, Greco J, Mui K, Aminipour S, Kim J, Fuller R, Rataj E, Lentz M, Sehgal P, Westmoreland S, de Crespigny A, Gonzalex R (2003) Diffusion MR detection of early white matter changes in the SIV primate model of neuroaids. Intl Soc Mag Reson Med, 2536

Hein A, Schuh H, Thiel S, Martin JP, Dorries R (2003) Ramified feline microglia selects for distinct variants of feline immunodeficiency virus during early central nervous system infection. J Neurovirol 9:465–476

Hokanson RM, TerWee J, Choi IS, Coates J, Dean H, Reddy DN, Wolf AM, Collisson EW (2000) Dose response studies of acute feline immunodeficiency virus PPR strain infection in cats. Vet Microbiol 76:311–327

Hopkins WG (2000) Measures of reliability in sports medicine and science. Sports Med 30:1–15

Laubenberger J, Haussinger D, Bayer S, Thielemann S, Schneider B, Mundinger A, Hennig J, Langer M (1996) HIV-related metabolic abnormalities in the brain: depiction with proton MR spectroscopy with short echo times. Radiology 199:805–810

Le Bihan D, Breton E, Lallemand D, Grenier P, Cabanis E, Laval-Jeantet M (1986) MR imaging of intravoxel incoherent motions: application to diffusion and perfusion in neurologic disorders. Radiology 161:401–407

Lentz MR, Kim JP, Westmoreland SV, Greco JB, Fuller RA, Ratai EM, He J, Sehgal PK, Halpern EF, Lackner AA, Masliah E, Gonzalez RG (2005) Quantitative neuropathologic correlates of changes in

ratio of N-acetylaspartate to creatine in macaque brain. Radiology 235:461–468

Lentz MR, Lee V, Westmoreland SV, Ratai EM, Halpern EF, Gonzalez RG (2008a) Factor analysis reveals differences in brain metabolism in macaques with SIV/AIDS and those with SIV-induced encephalitis. NMR Biomed 21:878–887

Lentz MR, Westmoreland SV, Lee V, Ratai EM, Halpern EF, Gonzalez RG (2008b) Metabolic markers of neuronal injury correlate with SIV CNS disease severity and inoculum in the macaque model of neuroAIDS. Magn Reson Med 59:475–484

Marcus CD, Taylor-Robinson SD, Sargentoni J, Ainsworth JG, Frize G, Easterbrook PJ, Shaunak S, Bryant DJ (1998) 1H MR spectroscopy of the brain in HIV-1-seropositive subjects: evidence for diffuse metabolic abnormalities. Metab Brain Dis 13:123–136

Mascalchi M, Filippi M, Floris R, Fonda C, Gasparotti R, Villari N (2005) Diffusion-weighted MR of the brain: methodology and clinical application. Radiol Med 109:155–197

McArthur JC, Hoover DR, Bacellar H, Miller EN, Cohen BA, Becker JT, Graham NM, McArthur JH, Selnes OA, Jacobson LP et al (1993) Dementia in AIDS patients: incidence and risk factors. Multicenter AIDS Cohort Study. Neurology 43:2245–2252

McArthur JC, McDermott MP, McClernon D, St Hillaire C, Conant K, Marder K, Schifitto G, Selnes OA, Sacktor N, Stern Y, Albert SM, Kieburtz K, deMarcaida JA, Cohen B, Epstein LG (2004) Attenuated central nervous system infection in advanced HIV/AIDS with combination antiretroviral therapy. Arch Neurol 61:1687–1696

Meeker RB (2007) Feline immunodeficiency virus neuropathogenesis: from cats to calcium. J Neuroimmune Pharmacol 2:154–170

Meyerhoff DJ, Weiner MW, Fein G (1996) Deep gray matter structures in HIV infection: a proton MR spectroscopic study. AJNR Am J Neuroradiol 17:973–978

Muller-Oehring EM, Schulte T, Rosenbloom MJ, Pfefferbaum A, Sullivan EV (2010) Callosal degradation in HIV-1 infection predicts hierarchical perception: a DTI study. Neuropsychologia 48:1133–1143

Pedersen NC, Leutenegger CM, Woo J, Higgins J (2001) Virulence differences between two field isolates of feline immunodeficiency virus (FIV-APetaluma and FIV-CPGammar) in young adult specific pathogen free cats. Vet Immunol Immunopathol 79:53–67

Pfefferbaum A, Rosenbloom MJ, Rohlfing T, Kemper CA, Deresinski S, Sullivan EV (2009) Frontostriatal fiber bundle compromise in HIV infection without dementia. AIDS 23:1977–1985

Phillips TR, Prospero-Garcia O, Wheeler DW, Wagaman PC, Lerner DL, Fox HS, Whalen LR, Bloom FE, Elder JH, Henriksen SJ (1996) Neurologic dysfunctions caused by a molecular clone of feline immunodeficiency virus, FIV-PPR. J Neurovirol 2:388–396

Phillips TR, Billaud JN, Henriksen SJ (2000) Methamphetamine and HIV-1: potential interactions and the use of the FIV/cat model. J Psychopharmacol 14:244–250

Phipps AJ, Hayes KA, Buck WR, Podell M, Mathes LE (2000) Neurophysiologic and immunologic abnormalities associated with feline immunodeficiency virus molecular clone FIV-PPR DNA inoculation. J Acquir Immune Defic Syndr 23:8–16

Podell M, Oglesbee M, Mathes L, Krakowka S, Olmstead R, Lafrado L (1993) AIDS-associated encephalopathy with experimental feline immunodeficiency virus infection. J Acquir Immune Defic Syndr 6:758–771

Podell M, Hayes K, Oglesbee M, Mathes L (1997) Progressive encephalopathy associated with CD4/CD8 inversion in adult FIV-infected cats. J Acquir Immune Defic Syndr Hum Retrovirol 15:332–340

Podell M, Maruyama K, Smith M, Hayes KA, Buck WR, Ruehlmann DS, Mathes LE (1999) Frontal lobe neuronal injury correlates to altered function in FIV-infected cats. J Acquir Immune Defic Syndr 22:10–18

Poli A, Pistello M, Carli MA, Abramo F, Mancuso G, Nicoletti E, Bendinelli M (1999) Tumor necrosis factor-alpha and virus expression in the central nervous system of cats infected with feline immunodeficiency virus. J Neurovirol 5:465–473

Pomara N, Crandall DT, Choi SJ, Johnson G, Lim KO (2001) White matter abnormalities in HIV-1 infection: a diffusion tensor imaging study. Psychiatry Research-Neuroimaging 106:15–24

Pomper MG, Sacktor N (2007) New techniques for imaging human immunodeficiency virus associated cognitive impairment in the era of highly active antiretroviral therapy. Arch Neurol 64:1233–1235

Power C, Buist R, Johnston JB, Del Bigio MR, Ni W, Dawood MR, Peeling J (1998a) Neurovirulence in feline immunodeficiency virus-infected neonatal cats is viral strain specific and dependent on systemic immune suppression. J Virol 72:9109–9115

Power C, McArthur JC, Nath A, Wehrly K, Mayne M, Nishio J, Langelier T, Johnson RT, Chesebro B (1998b) Neuronal death induced by brain-derived human immunodeficiency virus type 1 envelope genes differs between demented and nondemented AIDS patients. J Virol 72:9045–9053

Ragin AB, Storey P, Cohen BA, Epstein LG, Edelman RR (2004) Whole brain diffusion tensor imaging in HIV-associated cognitive impairment. American Journal of Neuroradiology 25:195–200

Ragin AB, Wu Y, Storey P, Cohen BA, Edelman RR, Epstein LG (2005) Diffusion tensor imaging of subcortical brain injury in patients infected with human immunodeficiency virus. J Neurovirol 11:292–298

Ratai EM, Pilkenton SJ, Greco JB, Lentz MR, Bombardier JP, Turk KW, He J, Joo CG, Lee V, Westmoreland S, Halpern E, Lackner AA, Gonzalez RG (2009) In vivo proton magnetic resonance spectroscopy reveals region specific metabolic responses to SIV infection in the macaque brain. BMC Neurosci 10:63

Ratai EM, Bombardier JP, Joo CG, Annamalai L, Burdo TH, Campbell J, Fell R, Hakimelahi R, He J, Autissier P, Lentz MR, Halpern EF, Masliah E, Williams KC, Westmoreland SV, Gonzalez RG (2010) Proton magnetic resonance spectroscopy reveals neuroprotection by oral minocycline in a nonhuman primate model of accelerated NeuroAIDS. PLoS One 5:e10523

Sacktor N, Skolasky RL, Ernst T, Mao X, Selnes O, Pomper MG, Chang L, Zhong K, Shungu DC, Marder K, Shibata D, Schifitto G, Bobo L, Barker PB (2005) A multicenter study of two magnetic resonance spectroscopy techniques in individuals with HIV dementia. J Magn Reson Imaging 21:325–333

Stebbins GT, Smith CA, Bartt RE, Kessler HA, Adeyemi OM, Martin E, Cox JL, Bammer R, Moseley ME (2007) HIV-associated alterations in normal-appearing white matter: a voxel-wise diffusion tensor imaging study. J Acquir Immune Defic Syndr 46:564–573

Steigerwald ES, Sarter M, March P, Podell M (1999) Effects of feline immunodeficiency virus on cognition and behavioral function in cats. J Acquir Immune Defic Syndr Hum Retrovirol 20:411–419

Tarasow E, Wiercinska-Drapalo A, Kubas B, Dzienis W, Orzechowska-Bobkiewicz A, Prokopowicz D, Walecki J (2003) Cerebral MR spectroscopy in neurologically asymptomatic HIV-infected patients. Acta Radiol 44:206–212

Tolnay AE, Baskin CR, Tumpey TM, Sabourin PJ, Sabourin CL, Long JP, Pyles JA, Albrecht RA, Garcia-Sastre A, Katze MG, Bielefeldt-Ohmann H (2010) Extrapulmonary tissue responses in cynomolgus macaques (Macaca fascicularis) infected with highly pathogenic avian influenza A (H5N1) virus. Arch Virol 155(6):905–914

Usiskin SI, Bainbridge A, Miller RF, Jager HR (2007) Progressive multifocal leukoencephalopathy: serial high-b-value diffusion-weighted MR imaging and apparent diffusion coefficient meas-

urements to assess response to highly active antiretroviral therapy. AJNR Am J Neuroradiol 28:285–286

Wenserski F, von Giesen HJ, Wittsack HJ, Aulich A, Arendt G (2003) Human immmunodeficiency virus 1-associated minor motor disorders: perfusion-weighted MR imaging and H-1 MR spectroscopy. Radiology 228:185–192

Wilkinson ID, Miller RF, Miszkiel KA, Paley MN, Hall-Craggs MA, Baldeweg T, Williams IG, Carter S, Newman SP, Kendall BE, Catalan J, Chinn RJ, Harrison MJ (1997) Cerebral proton magnetic resonance spectroscopy in asymptomatic HIV infection. AIDS 11:289–295

Williams K, Westmoreland S, Greco J, Ratai E, Lentz M, Kim WK, Fuller RA, Kim JP, Autissier P, Sehgal PK, Schinazi RF, Bischofberger N, Piatak M, Lifson JD, Masliah E, Gonzalez RG (2005) Magnetic resonance spectroscopy reveals that activated monocytes contribute to neuronal injury in SIV neuro-AIDS. J Clin Invest 115:2534–2545

Wu Y, Storey P, Cohen BA, Epstein LG, Edelman RR, Ragin AB (2006) Diffusion alterations in corpus callosum patients with HIV. American Journal of Neuroradiology 27:656–660

Yoon JH, Bang OY, Kim HS (2007) Progressive multifocal leukoencephalopathy in AIDS: proton MR spectroscopy patterns of asynchronous lesions confirmed by serial diffusion-weighted imaging and apparent diffusion coefficient mapping. Journal of Clinical Neurology 3:200–203